Effect of aberrations in a holographic system on reflecting volume Bragg gratings

Marc SeGall,* Daniel Ott, Ivan Divliansky, and Leonid B. Glebov

CREOL—The College of Optics & Photonics, University of Central Florida, P.O. Box 162700, Orlando, Florida 32816-2700, USA

*Corresponding author: msegall@creol.ucf.edu

Received 9 August 2013; revised 10 October 2013; accepted 14 October 2013;
posted 15 October 2013 (Doc. ID 195514); published 8 November 2013

The effect of aberrations in the recording beams of a holographic setup is discussed regarding the deterioration of properties of a reflecting volume Bragg grating. Imperfect recording beams result in a spatially varying grating vector, which causes broadening, asymmetry, and washed out side lobes in the reflection spectrum as well as a corresponding reduction in peak diffraction efficiency. These effects are more significant for gratings with narrower spectral widths. © 2013 Optical Society of America

OCIS codes: (090.2880) Holographic interferometry; (050.7330) Volume gratings; (220.1010) Aberrations (global).

http://dx.doi.org/10.1364/AO.52.007826

1. Introduction

Reflecting Bragg gratings (RBGs) are used as spectrally selective elements in a variety of applications including spectral beam combining [1,2], mode selection in lasers [3,4], and spectral filtering [4–7]. For applications requiring narrow spectral selectivity [8], or large apertures [9], these gratings must have a uniform period throughout the thickness of the recording medium, which may be on the order of millimeters, two orders of magnitude thicker than typical film gratings. In addition, this homogeneity in period must also exist over an aperture of several millimeters, which is one to two orders of magnitude larger than typical fibers. It has been shown that typical recording techniques such as holographic recording and recording through a phase mask can create an imperfect grating structure due to aberrations induced by the optics in the system [10,11]. However, to the best of our knowledge no one has characterized the deterioration in spectral response of such larger aperture, thick gratings.

In this paper we develop a method for determining the effects of aberrations on large aperture gratings recorded in thick media. This method may be used in any two-beam recording system and can be easily generalized to systems with three or more beams, though here we will focus on single-sided two-beam recording. Previous works have considered the effects of aberrations in a single recording plane where the beams perfectly overlap. Such an approach is valid for thin media (on the order of tens of micrometers), but for thick recording media (on the order of several millimeters) there will be a significant shift in the positions of the recording beams relative to each other as they traverse the recording medium. Therefore, the fringe pattern produced will not be constant throughout the grating if one or both beams have a nonuniform wavefront. Such nonuniform gratings may have a wider spectral width, a shifted resonant wavelength, or other problems. It is imperative therefore to know what the effects of aberrations will have on the properties of the RBGs. Here we consider the spatially dependent change in period and its effect on the reflection spectra induced by this imperfect fringe pattern.

2. Theory

Let us consider two aberrated beams that interfere at a recording medium as shown in Fig. 1. The beams will create a grating structure with a periodicity

1559-128X/13/327826-06$15.00/0

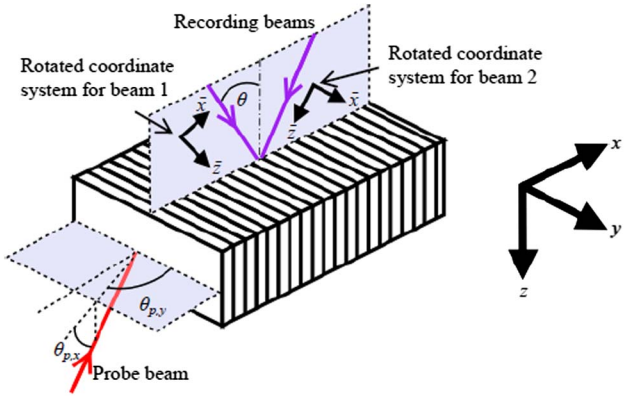

Fig. 1. Geometry of a grating recorded by two-beam interference where the nominal half angle of interference is θ. This grating acts as a reflecting grating for a probe beam incident in the plane orthogonal to the recording plane. All angles are angles inside the medium.

determined by the standard two-beam interference equation [12]:

$$I(x,y,z) = I_1 + I_2 + 2\sqrt{I_1 I_2}\cos((\vec{k}_1 - \vec{k}_2)\cdot\vec{r}), \quad (1)$$

where I is the intensity and $\vec{k}$ is the wavevector. In general, the wavevector for each beam is not a constant in the presence of aberrations. Therefore the wavevector at any given point must be determined from the local wavefront. To calculate the beam wavefront, let us consider one of the aberrated beams in the shifted coordinate system $(\bar{x},\bar{y},\bar{z})$, where the beam propagates along the $\bar{z}$ axis as in Fig. 1. (Note that this coordinate system is beam-specific.) In order to properly describe the aberrations of this beam, the aberrations at the $\bar{z}=0$ plane are written in terms of Zernike polynomials, which allow characterization the aberrations of the recording beam with a unique, orthogonal expansion [13–16]. As the Zernike polynomials are normalized to the radius r of the aperture of interest, the normalized dimensions are denoted as $(\bar{x}',\bar{y}') = (\bar{x},\bar{y})/r$. The electric field of the beam may then be written as

$$E(\bar{x},\bar{y},0) = E_0(\bar{x},\bar{y},0)\exp\left(ik\sum_n Z_n(\bar{x}',\bar{y}')\right), \quad (2)$$

where Z_n is the nth Zernike polynomial in Noll notation [13]. While this characterization is sufficient for thin gratings, the beam must be propagated through the depth of the recording medium for thick gratings. Therefore the three-dimensional distribution of the electric field is calculated using the beam propagation method:

$$E(\bar{x},\bar{y},\bar{z}) = \mathcal{F}^{-1}\left\{\mathcal{F}\{E(\bar{x},\bar{y},0)\}e^{\frac{-(f_x^2+f_y^2)\bar{z}}{2k}}\right\}e^{ik\bar{z}}. \quad (3)$$

As the local phase incursion φ of the electric field at a given $\bar{z}$-plane is related to the wavefront by $\varphi = k(\bar{z}+W)$, the wavefront at a given $\bar{z}$-plane may be calculated by

$$W(\bar{x},\bar{y},\bar{z}) = \frac{1}{k}\arctan\left(\frac{\mathrm{Im}[E(\bar{x},\bar{y},\bar{z})]}{\mathrm{Re}[E(\bar{x},\bar{y},\bar{z})]}\right) - \bar{z}. \quad (4)$$

The local wavevector is then given by the gradient of the wavefront:

$$\vec{k}(\bar{x},\bar{y},\bar{z}) = \frac{k}{\sqrt{1+\left(\frac{\partial W}{\partial \bar{x}}\right)^2+\left(\frac{\partial W}{\partial \bar{y}}\right)^2}}\begin{pmatrix}-\frac{\partial W}{\partial \bar{x}}\\ -\frac{\partial W}{\partial \bar{y}}\\ 1\end{pmatrix}. \quad (5)$$

In order to calculate the wavevector in the grating-centered coordinate system, we must convert the local wavevector from the beam-centered coordinate system to the original (x,y,z) coordinate system by rotating by the half angle of interference θ:

$$\vec{k}_g(\bar{x},\bar{y},\bar{z}) = \begin{pmatrix}\cos\theta & 0 & \sin\theta\\ 0 & 1 & 0\\ -\sin\theta & 0 & \cos\theta\end{pmatrix}\vec{k}(\bar{x},\bar{y},\bar{z}). \quad (6)$$

Finally, the position of the local wavevector along the wavefront in the (x,y,z) coordinate system is given by converting the $(\bar{x},\bar{y},\bar{z})$ coordinates to (x,y,z) coordinates, giving

$$\vec{k}_g(x\cos\theta - z\sin\theta, y, -x\sin\theta + z\cos\theta) = \vec{k}_g(\bar{x},\bar{y},\bar{z}). \quad (7)$$

In situations where the intensity distribution of a recording beam is altered due to aberrations such as strong defocus, the fact that a particular wavefront in the $(\bar{x},\bar{y},\bar{z})$ coordinate system does not cross a given z-plane all at once must be considered. To take this into account, it is necessary in general to propagate the beam until all of the local wavevectors are known at a given plane. However, this is an atypical case and the aberrations in a typical recording beam are expected to be small enough that the beam should still behave similar to a plane wave. Therefore the amount of spatial deviation of the wavefront after propagating a few millimeters is expected to be negligible and a local wavevector will therefore travel parallel to the tilt angle of the recording beam. In this case the wavevector at the $z=0$ plane can be written as

$$\vec{k}_g(x,y,0) = \vec{k}_g(\bar{x}/\cos\theta_{\mathrm{eff},x}, \bar{y}/\sin\theta_{\mathrm{eff},y}, 0), \quad (8)$$

and the wavevector at an arbitrary z-plane can be written as

$$\vec{k}_g(x,y,z) = \vec{k}_g(x + z\tan\theta_{\mathrm{eff},x}, y + z\cot\theta_{\mathrm{eff},y}, 0). \quad (9)$$

Here the effective angles are given by

$$\theta_{\text{eff},x} = \arctan\left(\frac{\vec{k}_{g,x}(0,0,0)}{\vec{k}_{g,z}(0,0,0)}\right)$$

$$\theta_{\text{eff},y} = \arccos\left(\frac{\vec{k}_{g,y}(0,0,0)}{k}\right), \tag{10}$$

where it should be noted that $\theta_{\text{eff},y}$ is given using the standard notation for spherical coordinates. The effective angles take into account the half angle of rotation as well as any alterations to the half angle caused by tilt. The resulting grating recorded by these local wavevectors will have a local period as well as local tilt, as illustrated in Fig. 2.

If the probe beam were incident on the same face as the recording beams, the grating would act as a transmitting grating, with a local grating vector of

$$\vec{K}_{\text{TBG}}(x,y,z) = \vec{k}_{g,1}(x,y,z) - \vec{k}_{g,2}(x,y,z). \tag{11}$$

However, to use the grating as a reflecting grating, the probe beam must be incident from a perpendicular plane as shown in Fig. 1, which requires an additional 90° rotation:

$$\vec{K}_{\text{RBG}} = \begin{pmatrix} 0 & 0 & -1 \\ 0 & 1 & 0 \\ 1 & 0 & 0 \end{pmatrix} \vec{K}_{\text{TBG}} \tag{12}$$

for a probe beam incident along the x axis. The local grating tilt is then $\tan\phi_x = K_x/K_z$ and $\cos\phi_y = K_y/K$.

To determine the reflection spectrum of the grating for a probe beam propagating along the x axis we may first determine the reflection spectrum at a single point and then integrate all spectra over the grating aperture (defined as the y–z plane for the probe beam):

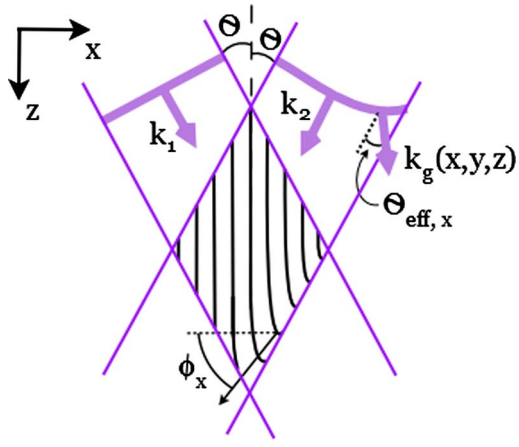

Fig. 2. One-dimensional illustration of a grating recorded by two beams incident at local angles $\theta_{\text{eff},x}$. The local wavevector in the aberrated wavefront creates a local grating period and a local tilt angle ϕ_x

$$R(\lambda) = \frac{\iint R(y,z,\lambda) I_p(y,z,\lambda)\,\mathrm{d}y\mathrm{d}z}{\int I_p(y,z,\lambda)\,\mathrm{d}y\mathrm{d}z}. \tag{13}$$

Here R is the reflectance and I_p is the intensity of the probe beam being reflected by the volume grating. However, because the grating has a spatially dependent period and inclination factor, we utilize the coupled-wave theory transfer matrix technique [17] to calculate the reflection at a given wavelength.

Coupled-wave theory dictates that the fields of forward and backward propagating waves in a uniform grating can be written as follows:

$$\begin{pmatrix} E_+(0) \\ E_-(0) \end{pmatrix} = \mathbf{T} \begin{pmatrix} E_+(t) \\ E_-(t) \end{pmatrix}. \tag{14}$$

Here E_+ and E_- are the forward and backward propagating waves, respectively, and $\mathbf{T}$ is a transfer matrix with elements

$$\begin{aligned} T_{11} &= [\cosh(\gamma t) + i\Delta k\, \sinh(\gamma t)/\gamma]\exp(ik_{\text{Bragg}}t) \\ T_{12} &= -\kappa t\, \sinh(\gamma t)\exp(-i(k_{\text{Bragg}}t + \zeta))/(\gamma t) \\ T_{21} &= -\kappa t\, \sinh(\gamma t)\exp(i(k_{\text{Bragg}}t + \zeta))/(\gamma t) \\ T_{22} &= [\cosh(\gamma t) - i\Delta k\, \sinh(\gamma t)/\gamma]\exp(-ik_{\text{Bragg}}t). \end{aligned} \tag{15}$$

Here $\Delta k = k_p - k_{\text{Bragg}}$ is the difference between the propagation constant of the probe beam and the propagation constant for a wave satisfying the Bragg condition, ζ is the grating phase factor, $\kappa = \pi\delta n/\lambda$ is the coupling coefficient between the forward and backward-propagating waves (assuming TE polarization), $\gamma^2 = \kappa^2 - (\Delta k)^2$, and δn is the refractive index modulation [17,18].

In order to determine the k_{Bragg} term, the general case of grating tilt must be considered in which there is a y component to the grating tilt as well as an x component. It is therefore necessary to generalize Kogelnik's coupled-wave equations to cases where the grating vector does not lie in the x–z plane. Using [18] as a template and assuming that the y component of the grating and probe beam vectors are nonzero, we find that the Bragg condition becomes

$$K = 2k_{\text{Bragg}}(\sin\theta_y \sin\phi_y \cos(\phi_x - \theta_x) + \cos\theta_y \cos\phi_y), \tag{16}$$

where θ_x and ϕ_x are the angles of the probe beam and grating vectors, respectively, relative to the x axis (as the x axis is the axis for which the probe beam nominally propagates along), and θ_y and ϕ_y are the angles of the probe beam and grating vectors, respectively, relative to the y axis. Note that in this formulation we use the standard spherical coordinate definitions for the angles, so a grating vector that lies in the x–z plane has an inclination angle of $\phi_y = \pi/2$, reducing Eq. (16) to the Bragg condition described by Kogelnik.

Note also that each of the terms in Eq. (15) is assumed to be constant. To allow for a varying period

and grating tilt we will assume the slowly varying envelope approximation, permitting us to divide the grating into N segments and write $\mathbf{T}$ as

$$\mathbf{T} = \prod_{i=1}^{N} \mathbf{T}_i, \tag{17}$$

where $\mathbf{T}_i$ is a function of a local (constant) κ_i, Δk_i, t_i and ζ_i. In order to match the phases between the segments, ζ_i must satisfy the relationship $\zeta_i = \zeta_{i-1} + 2t_{i-1}\pi/\Lambda_{i-1}$ [17]. The reflectance at a given point is then given by

$$R(y, z, \lambda) = \left| \frac{T_{21}}{T_{11}} \right|^2. \tag{18}$$

Inserting Eq. (18) into Eq. (13) provides the reflection spectrum for a probe beam incident upon the front facet of a grating.

3. Modeling

Because of the spatially varying nature of the grating, one may reasonably conclude that several factors will influence the reflection spectrum, including the thickness and refractive index modulation of the grating, the position of the probe beam along the grating face, and the size of the probe beam. The combination of grating and beam parameters provides a plethora of possible deteriorated profiles. To demonstrate the influence of these effects we simulate two gratings representing different applications for lasers emitting in the vicinity of 1064 nm. The first one is a high efficiency, relatively thin grating (Grating A), useful in applications such as spectral beam combining, and the second one is a thick grating with moderate diffraction efficiency (Grating B), which may be used in applications requiring narrow spectral widths. A recording medium that is capable of recording such large-aperture, thick gratings is photo-thermo-refractive glass, which has been demonstrated in a variety of applications [19]. This glass is transparent in the visible and NIR range and photosensitive in the near UV region. One of the most common recording wavelengths for this glass is the emission wavelength 325 nm, the emission wavelength of a He–Cd laser.

Grating A is designed such that it ideally has a 1064 nm resonant wavelength with $\delta n = 200$ ppm and $t = 5.5$ mm. From Eqs. (13) to (18) this should give a peak diffraction efficiency of 99.4% and a spectral width of 178 pm (FWHM). Grating B is designed for the same resonant wavelength, with $\delta n = 20$ ppm, and $t = 20$ mm, corresponding to a diffraction efficiency of 68.5% and a spectral width of 24 pm. To account for beam size and position, a 3 mm diameter Gaussian probe beam at normal incidence is used for modeling. Two locations along the grating aperture are examined: the center of the grating where the effects of aberrations are expected to be minimal and halfway between the grating edge and center along the y axis. For 25 mm diameter recording beams interfering through a 6 mm deep recording medium (z-axis dimension), the probe locations correspond to $y = 0$ and $y = 6.25$ mm with $z = 0$ in the $y - z$ plane.

To observe the effects of one wave (peak-to-valley) of a given aberration we have calculated the transfer matrix by dividing Grating A into 100 segments along the x axis and Grating B into 500 segments so that each segment is approximately 50 μm. To minimize the effects of any possible grating chirp, Grating A was analyzed over the region $x = -2.75$ mm to $x = 2.75$ mm and Grating B was analyzed over the region $x = -10$ mm to $x = 10$ mm. Figures 3(a) and 3(b) show the effects of one wave of a given aberration at the recording wavelength of 325 nm on the reflectance spectrum at 1064 nm for Grating A and Figs. 3(c) and 3(d) show the effects for Grating B in the presence of the first several terms of the wavefront expansion (where the terms are defined as in [13]). In Figs. 3(a) and 3(c), the probe beam was centered on the grating and in Figs. 3(b) and 3(d) the probe beam was halfway between the center and edge of the grating along the y axis.

A comparison of these figures shows four commonly occurring effects: a shift in resonant wavelength, side lobes becoming at least partially washed out, a reduction of peak diffraction efficiency, and spectral broadening. Defocus and spherical aberrations show similar behavior for both gratings simulated, with the resonant wavelength being unaffected but the side lobes becoming washed out and the peak diffraction efficiency being reduced, with Grating B showing a far more pronounced reduction than Grating A. This difference in peak diffraction efficiency reduction between the two gratings can be attributed to the difference in the initial spectral widths of the gratings. Because Grating A has a wide initial spectral width, small deviations in the reflectance spectra at individual points are masked, whereas in Grating B these deviations constitute a significant shift relative to the spectral acceptance of the grating and therefore have a more noticeable effect in the integrated spectrum, resulting in reduced peak diffraction efficiency and spectral broadening.

45° astigmatism shows behavior similar to defocus and spherical when the probe beam is centered on the grating, but when it is moved off-center there is a change in resonant wavelength as well. This shift in resonant wavelength is identical for both gratings, but since Grating B has a narrower spectral acceptance, the shifted spectrum falls almost entirely outside of the desired spectral region, whereas there is still a region of overlap in Grating A. Coma x likewise displays a shifted resonant wavelength, even when the probe beam is centered on the grating, and in addition the spectra are asymmetrical, similar to chirped gratings [20]. The effects of coma x are most noticeable, however, in Grating B, where spectral broadening has completely deformed the reflectance spectrum.

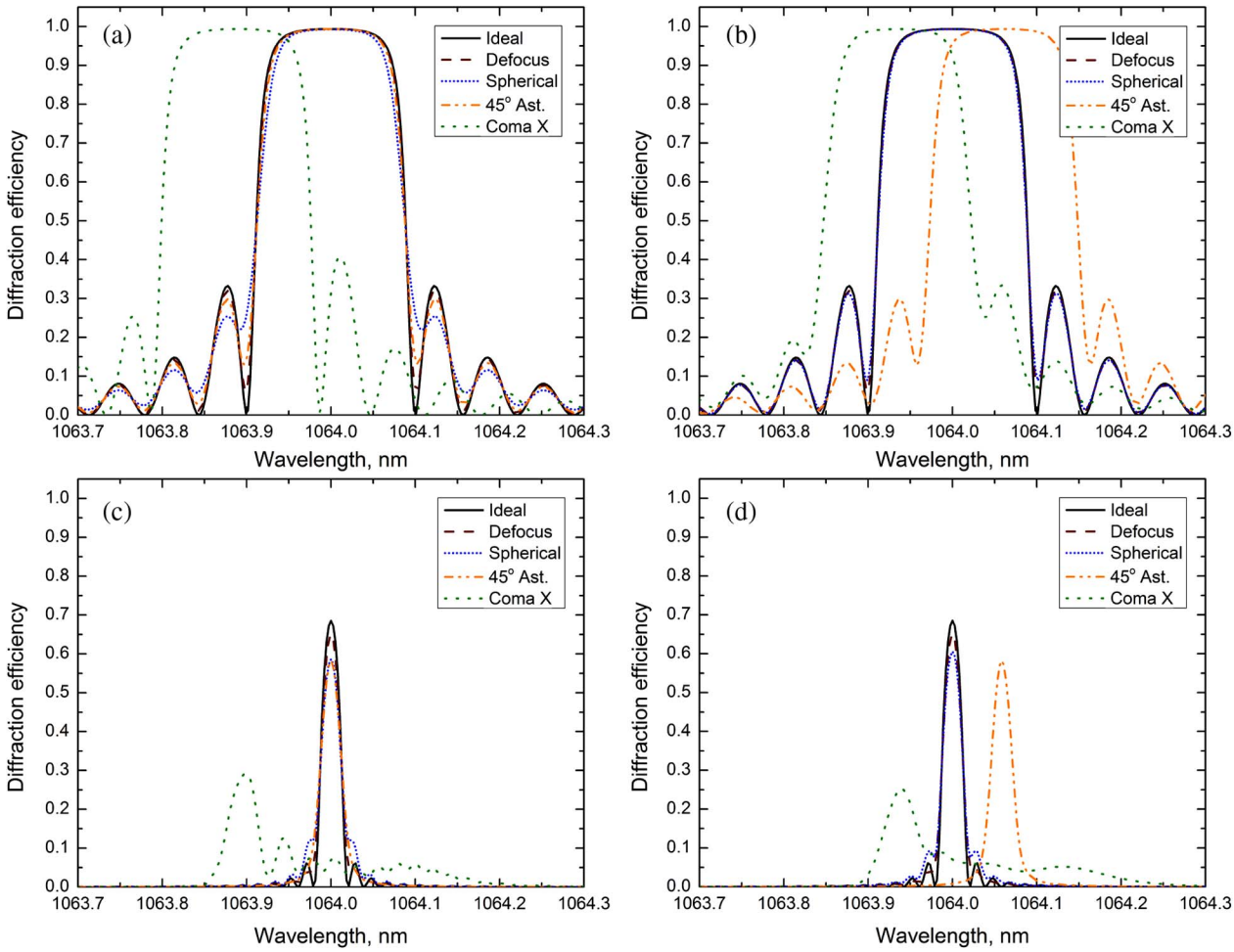

Fig. 3. Reflection spectra in the presence of one wave of a given aberration for [(a), (b)] Grating A and [(c), (d)] Grating B. The probe beam is incident at [(a), (c)] the center of the grating and [(b), (d)] halfway between the center and the edge of the grating.

As mentioned previously, the degradation in spectral profiles is a combination of local differences in resonant wavelength as well as the local differences in grating tilt at individual points, which, when integrated into the full spectrum, result in the above effects. We would like to stress here that both the differences in grating tilt and resonant wavelength must be considered in order to properly characterize the deteriorated spectra. If for instance the deviations in local grating tilt are ignored, the deteriorated spectra will still show spectral broadening, a shift of resonant wavelength, etc., but the overall profile will be significantly different from the profiles calculated by taking both effects into account [21]. Thus in order to properly characterize the effects of aberrations on the reflectance spectra of a volume Bragg grating, the above methodology should be used.

4. Conclusions

We have developed a numerical method to characterize the effects of aberrations in a holographic recording system on RBGs, which can be used in any recording geometry and for any combination of aberrations and grating parameters. Aberrations in recording beams can have potentially significant adverse effects on properties of thick RBGs due to the spatial dependence of the overlapped wavefronts. This results local deviations in the grating vector, causing effects such as a spatially varying resonant wavelength, which is problematic for spectral filtering, and washed out sides lobes of the reflection spectrum, which reduces the combining efficiency of spectral beam combining using dense channel spacing. Asymmetrical spectra, spectral broadening, and a reduction in peak diffraction efficiency may also be present, though the wider the initial spectral width, the less noticeable these effects will be.

This work was supported in part by HEL JTO contract W911NF-10-1-0441. We would like to thank the University of Central Florida Stokes Advanced Research Computing Center for providing computational resources and support.

References

1. A. Sevian, O. Andrusyak, I. Ciapurin, V. Smirnov, G. Venus, and L. Glebov, "Efficient power scaling of laser radiation by spectral beam combining," Opt. Lett. **33**, 384–386 (2008).
2. O. Andrusyak, V. Smirnov, G. Venus, V. Rotar, and L. Glebov, "Spectral combining and coherent coupling of lasers by

volume Bragg gratings," IEEE J. Sel. Top. Quantum Electron. **15**, 344–353 (2009).
3. Z. Sun, Q. Li, H. Lei, Y. Hui, and M. Jiang, "Sub-nanosecond pulse, single longitudinal mode Q-switched Nd:YVO_4 laser controlled by reflecting Bragg gratings," Opt. Laser Technol. **48**, 475–479 (2013).
4. D. Ott, V. Rotar, J. Lumeau, S. Mokhov, I. Divliansky, A. Ryasnyanskiy, N. Vorobiev, V. Smirnov, C. Spiegelberg, and L. Glebov, "Longitudinal mode selection in laser cavity by moiré volume Bragg grating," Proc. SPIE **8236**, 823621 (2012).
5. J. Lumeau, L. B. Glebov, and V. Smirnov, "Tunable narrow-band filter based on a combination of Fabry–Perot etalon and volume Bragg grating," Opt. Lett. **31**, 2417–2419 (2006).
6. V. Smirnov, J. Lumeau, S. Mokhov, B. Ya. Zeldovich, and L. B. Glebov, "Ultranarrow bandwidth moiré reflecting Bragg gratings recorded in photo-thermo-refractive glass," Opt. Lett. **35**, 592–594 (2010).
7. J. Lumeau, C. Koc, O. Mokhun, V. Smirnov, M. Lequime, and L. B. Glebov, "Single resonance monolithic Fabry–Perot filters formed by volume Bragg gratings and multilayer dielectric mirrors," Opt. Lett. **36**, 1773–1775 (2011).
8. T. Hieta, M. Vainio, C. Moser, and E. Ikonen, "External-cavity lasers based on a volume holographic grating at normal incidence for spectroscopy in the visible range," Opt. Commun. **282**, 3119–3123 (2009).
9. J. Saikawa, M. Fujii, H. Ishizuki, and T. Taira, "High-energy, narrow-bandwidth periodically poled Mg-doped $LiNbO_3$ optical parametric oscillator with a volume Bragg grating," Opt. Lett. **32**, 2996–2998 (2007).
10. N. Chen, "Aberrations of volume holographic grating," Opt. Lett. **10**, 472–474 (1985).
11. M. Ma, X. Wang, and F. Wang, "Aberration measurement of projection optics in lithographic tools based on two-beam interference theory," Appl. Opt. **45**, 8200–8208 (2006).
12. R. S. Sirohi, *Optical Methods of Measurement: Wholefield Techniques*, 2nd ed. (CRC Press, 2009).
13. R. J. Noll, "Zernike polynomials and atmospheric turbulence," J. Opt. Soc. Am. **66**, 207–211 (1976).
14. J. Wyant and J. Creath, "Basic wavefront aberration theory for optical metrology," in *Applied Optics and Optical Engineering*, R. Shannon and J. Wyant, eds. (Academic, 1992), Vol. **XI**, pp. 1–53.
15. V. N. Mahajan, "Zernike polynomials and wavefront fitting," in *Optical Shop Testing*, D. Malacara, ed., 3rd ed. (Wiley, 2007), pp. 498–546.
16. G. Dai, *Wavefront Optics for Vision Correction* (SPIE, 2008).
17. M. Yamada and K. Sakuda, "Analysis of almost-periodic distributed feedback slab waveguides via a fundamental matrix approach," Appl. Opt. **26**, 3474–3478 (1987).
18. H. Kogelnik, "Coupled wave theory for thick volume holograms," Bell Syst. Tech. J. **48**, 2909–2947 (1969).
19. L. B. Glebov, "Volume holographic elements in a photo-thermo-refractive glass," J. Holography Speckle **5**, 1–8 (2008).
20. R. R. A. Syms, *Practical Volume Holography*, Oxford Engineering Science Series (Clarendon, 1990), p. 24.
21. M. SeGall, D. Ott, I. Divliansky, and L. B. Glebov, "The effect of aberrated recording beams on reflecting Bragg gratings," Proc. SPIE **8644**, 864408 (2013).